Available online at www.sciencedirect.com
SCIENCE DIRECT®
ELSEVIER
Ultramicroscopy 103 (2005) 67–81
ultramicroscopy
www.elsevier.com/locate/ultramic

Conventional and back-side focused ion beam milling for off-axis electron holography of electrostatic potentials in transistors

Rafal E. Dunin-Borkowski[a,b,*], Simon B. Newcomb[c], Takeshi Kasama[a,b], Martha R. McCartney[d], Matthew Weyland[a], Paul A. Midgley[a]

[a]*Department of Materials Science and Metallurgy, University of Cambridge, Pembroke Street, Cambridge CB2 3QZ, UK*
[b]*RIKEN (The Institute of Physical and Chemical Research), 2-1 Hirosawa, Wako, Saitama 351-0198, Japan*
[c]*Sonsam Limited, Glebe Laboratories, Newport, Co. Tipperary, Ireland*
[d]*Center for Solid State Science, Arizona State University, Tempe, AZ 85287-1704, USA*

Abstract

Off-axis electron holography is used to characterize a linear array of transistors, which was prepared for examination in cross-sectional geometry in the transmission electron microscope (TEM) using focused ion beam (FIB) milling from the substrate side of the semiconductor device. The measured electrostatic potential is compared with results obtained from TEM specimens prepared using the more conventional 'trench' FIB geometry. The use of carbon coating to remove specimen charging effects, which result in electrostatic fringing fields outside 'trench' specimens, is demonstrated. Such fringing fields are not observed after milling from the substrate side of the device. Analysis of the measured holographic phase images suggests that the electrically inactive layer on the surface of each FIB-milled specimen typically has a thickness of 100 nm.

PACS: 61.14.Nm; 85.30.Pq

Keywords: Off-axis electron holography; Focused ion beam milling; Back-side milling; Electrostatic potential; Dopant contrast; Specimen preparation; Charging

1. Introduction

Off-axis electron holography is a powerful technique that is increasingly used to characterize electrostatic and magnetic fields in materials in the transmission electron microscope (TEM). The

*Corresponding author. Tel.: +44 1223 334564; fax: +44 1223 334567.
E-mail addresses: rafal.db@msm.cam.ac.uk (R.E. Dunin-Borkowski), simon@sonsam.ie (S.B. Newcomb), tk305@cam.ac.uk (T. Kasama), molly.mccartney@asu.edu (M.R. McCartney).

0304-3991/$ - see front matter © 2004 Elsevier B.V. All rights reserved.
doi:10.1016/j.ultramic.2004.11.018

basis of the technique, which is described in detail elsewhere (e.g., [1–3]), is illustrated schematically in the form of a ray diagram in Fig. 1. An electron biprism (typically, a sub-μm-diameter wire) is used to overlap the high-energy electron wave that has passed through the specimen with another part of the same electron wave that has passed only through vacuum. If a coherent, field emission electron source is used, then the local intensity and spacing of the interference fringes that form in the overlap region can be used to determine the amplitude and the phase shift, respectively, of the specimen electron wave. The phase shift ϕ is of particular interest for the characterization of semiconductor devices as it provides direct access to the electrostatic potential in the specimen (projected in the electron beam direction). The potential is, in turn, sensitive to the distribution of electrically active dopant atoms.

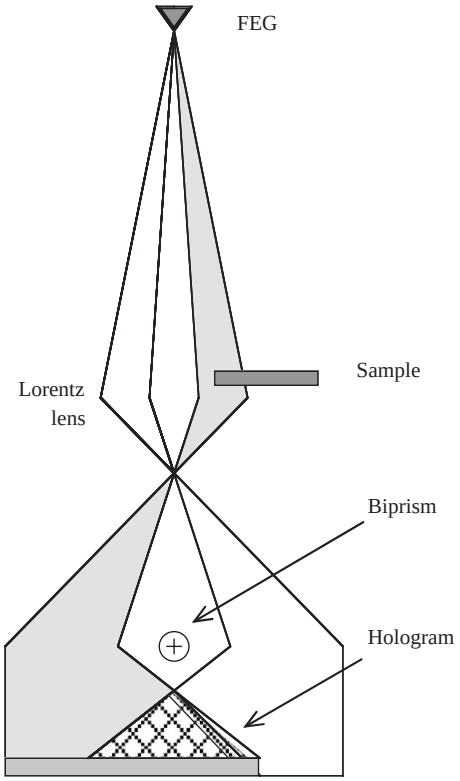

Fig. 1. Schematic illustration of setup used to generate off-axis electron holograms. The essential components are the field emission gun (FEG) electron source, which is used to provide coherent illumination, and the electrostatic biprism, which is used to cause overlap of the sample and reference waves. The Lorentz lens provides an optimal field of view and interference fringe spacing for electron holography of semiconductor devices.

For a non-magnetic material, in the absence of dynamical diffraction, ϕ can be related to the electrostatic potential in the specimen by the relation

$$\phi(x,y) = C_{\mathrm{E}} \int V(x,y,z)\,\mathrm{d}z, \tag{1}$$

where V is the potential, z is a direction parallel to (and x and y are directions perpendicular to) the incident electron beam, and C_{E} is a specimen-independent constant that takes a value of 7.3×10^6 rad/V m at a microscope accelerating voltage of 200 kV. If the potential V does not vary along z within a specimen of thickness t, then Eq. (1) can be simplified to

$$\phi(x,y) = C_{\mathrm{E}} V(x,y) t(x,y). \tag{2}$$

In a doped semiconductor, the primary contributions to V are from the mean inner potential V_0, which is related to the composition and density of the specimen, and from the space charge (or dopant) potential V_{d}, which is associated with longer-range charge redistribution due to local variations in dopant concentration [4]. (The step in potential across a p–n junction is then associated with a variation in V_{d} rather than V_0; this distinction is subjective, and it would also be possible to define the step in potential solely in terms of a variation in V_0). To a first approximation, these contributions to the phase shift can be included in Eq. (2) in the form

$$\phi(x,y) = C_{\mathrm{E}}[V_0(x,y)t(x,y) + V_{\mathrm{d}}(x,y)t_{\mathrm{el}}(x,y)], \tag{3}$$

where the dopant atoms are assumed to be electrically 'active' within specimen thickness t_{el}, which is smaller than the total specimen thickness t as a result of the combined effects of surface depletion and both damage and implantation due to specimen preparation. (These issues are discussed below.) A variation in either the mean inner potential or the space charge contribution to the potential (as well as beam-induced specimen charging) can, in principle, also result in the

presence of an electrostatic fringing field outside the specimen surface, in addition to the variation in potential within it.

Eqs. (1)–(3) suggest that the dopant potential in a semiconductor device can be revealed directly at a spatial resolution that can approach the nanometer scale by recording a phase image, in which n- and p-type regions exhibit bright and dark contrast, respectively. The potential of a Si specimen is expected to vary by approximately 1 V depending on the dopant concentration [4]. The ability to record such maps routinely, quantitatively and reliably is of interest to the semiconductor industry, which has a pressing need for high spatial resolution information about two- and three-dimensional dopant distributions for the evaluation of process parameters and for simulations of dopant diffusion.

However, it is increasingly recognized that TEM specimen preparation can have a profound influence on the electrostatic potential in a doped semiconductor, altering the measured potential from that in the original device. It is therefore important to assess the effect of different TEM specimen preparation techniques on dopant potentials measured using electron holography. In this paper, we concentrate on assessing the technique of focused ion beam (FIB) milling, which usually involves the use of 30 kV Ga ions to micro-machine a specimen to electron transparency. This technique is increasingly used to prepare site-specific regions of semiconductor devices for electron holography (e.g., [5–8]). However, the resulting combination of physical damage, implantation and doping of the specimen surface with Ga [9–11] can result in the modification of the electronic properties of the thin specimen [12,13]. The development of a specimen preparation procedure based on FIB milling that minimizes these effects is required urgently. A further problem with the use of FIB milling results from the fact that the recorded phase image depends on specimen thickness as well as on the dopant potential of interest. If a single milling direction is used, then thickness corrugations ('curtaining') in the doped semiconductor can result when regions of the specimen that have a lower sputtering yield block a material that has a faster sputtering yield. This artifact is particularly problematic for electron holography of device structures, which may have metallization layers on their surfaces. For Si, which has a mean inner potential of ~12 V, a variation of 2 nm (four unit cells) in the thickness of a 200-nm-thick specimen would result in the same phase change as a 0.1 V step in dopant potential in a specimen of uniform thickness.

All of these issues must be balanced with three more general limitations on the geometry and quality of a TEM specimen that are essential for off-axis electron holography. First, the region of interest must lie within 1–2 μm of vacuum in order to provide a reference wave that can be overlapped onto the specimen. Second, as well as being as uniform in thickness as possible, the specimen should be oriented to a weakly diffracting orientation to avoid the effects of diffraction contrast on the measured phase shift. Finally, charging of the specimen due to secondary electron emission in the TEM, which can result in band-bending, junction biasing and fringing fields that can perturb the vacuum reference wave, should be minimized.

In this paper, we assess some of these issues by using off-axis electron holography to characterize a Si device that contains four transistors, which are located below metallization layers. We obtain results from specimens that have been prepared using both conventional FIB milling and FIB milling from the substrate side of the wafer. Although several other, less invasive, TEM specimen preparation techniques have been used to prepare transistors for examination using electron holography (e.g., [14,15]), the advantages of FIB milling (in particular its site-specificity) suggest that this technique should be assessed in detail and developed. The results described here have been presented in preliminary form elsewhere [16].

2. Materials and methods

Four closely-spaced Si transistors, which were located 5 μm below the wafer surface and separated from it by metallization layers, were prepared for electron holography in several different geometries by using FIB milling in an

FEI FIB 200 workstation. Details of the specimen geometries and materials are given below. These transistors present a significant, but representative, challenge for TEM specimen preparation both because the metallization layers are substantial and likely to result in thickness corrugations in the doped regions of interest and because these overlayers must, at least in part, be removed to provide a vacuum reference wave for electron holography. An additional difficulty arises from the possibility that the overlayers, which contain silicon oxides, may charge during examination in the electron microscope.

Off-axis electron holograms of the transistors were recorded at 200 kV using a Philips CM200ST FEG TEM equipped with a Lorentz lens, a rotatable electron biprism (a 0.6-μm-diameter Au-coated quartz wire located in place of one of the conventional selected-area apertures), and a charge-coupled-device (CCD) camera located between the microscope viewing screen and the plate camera. Holograms were recorded with the Lorentz lens switched on and the conventional microscope objective lens switched off using an acquisition time of 4 s. The microscope magnification was 15k ×, corresponding to a field of view on the CCD camera of 1.26 μm. A positive voltage of 160 V applied to the biprism wire resulted in a holographic overlap width of 1.04 μm. The transistors were always oriented close to a weakly diffracting orientation a few degrees from the ⟨1 1 0⟩ zone axis of the Si substrate for electron holography. Digital analysis of the holograms to provide amplitude and phase images, using procedures that are described in detail elsewhere (e.g., [1]), was carried out using library programs written in the Semper image processing language [17]. A measure of the total (crystalline and amorphous) specimen thicknesses $t(x,y)$ in each doped region was always obtained in units of inelastic mean free path λ_{in} from holographic amplitude images $A(x,y)$ (after normalizing by the amplitudes of reference holograms) by using the equation [18]

$$\frac{t(x,y)}{\lambda_{in}} = -2 \ln A(x,y). \quad (4)$$

A value for λ_{in} of 85 nm in Si at 200 kV is generally accepted when using a Lorentz lens (e.g., [12]). Although this value of λ_{in} should strictly be a weighted average of that in the crystalline region of the specimen and in any amorphous layers on its surfaces, these values are expected to be similar.

3. Results

3.1. 'Trench' geometry

Fig. 2 illustrates schematically the conventional 'trench' FIB approach [19,20] used to prepare cross-sectional TEM specimens of the linear array of transistors in the present study. Each specimen was initially milled perpendicular to the wafer surface (Fig. 2a), using a beam current of 11 nA, after depositing a Pt protective strap. This step allowed the positions of the transistors to be located in the middle of a membrane whose thickness was at this stage greater than 1 μm. After repositioning the specimen in the FIB workstation, milling from the side was carried out, using an ion current of 350 pA, to remove the upper metallization layers (Fig. 2b). This step provided a region of vacuum within 1 μm of the doped regions of interest. After further repositioning, milling was again carried out perpendicular to the wafer surface (Fig. 2c), using an ion current of 150 pA, to leave an electron-transparent membrane whose thickness was now below 500 nm. Finally, two cuts were made in the sides of the membrane (Fig. 2d) in order to relieve strain, and the membrane surfaces were cleaned using low-angle Ar ion milling in a Gatan precision ion polishing system (PIPS). Care was taken to minimize implantation of Ga into the doped regions in the specimen, although some implantation is inevitable from the tails of the Gaussian profile of the incident ion beam.

Fig. 3 shows an FIB image of an intermediate stage of the milling procedure (corresponding to Fig. 2b). In this image, labels A, B, C and D correspond to PMOS (0.5 μm gate), PMOS (0.35 μm gate), NMOS (0.5 μm gate) and NMOS (0.35 μm gate) transistors, respectively. The bright bands above the transistors are W contacts, which are separated from each other by layers of amorphous Si oxide. The nominal dopant concentration in the

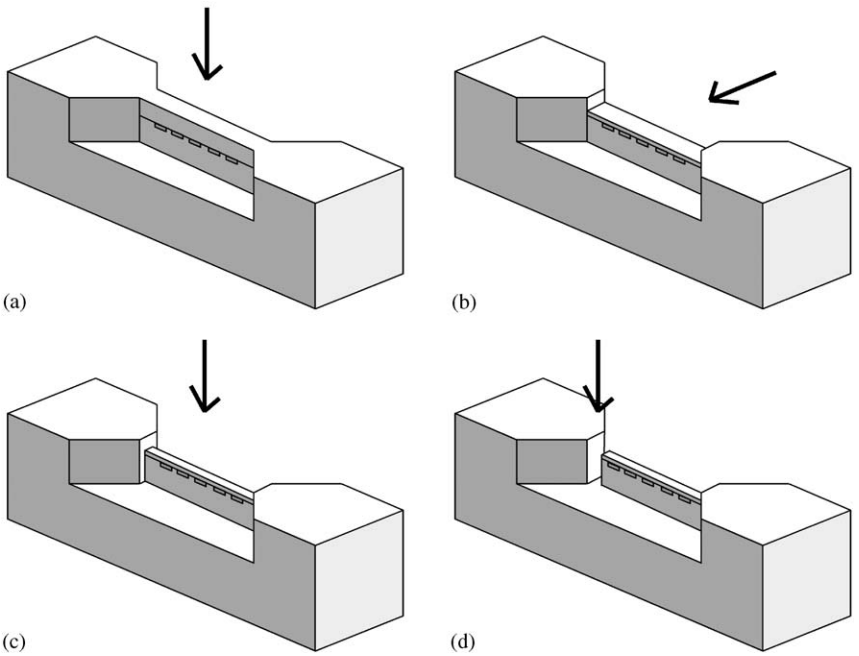

Fig. 2. Schematic diagrams illustrating the conventional 'trench' approach for preparing a cross-sectional TEM specimen of a linear array of transistors using FIB milling. The stages involved include: (a) initial milling from the top (perpendicular to the original wafer surface) to a membrane thickness of $>1\,\mu m$; (b) milling from the side using an ion current of 350 pA to remove the upper passivation and metallization layers on the wafer surface in order to provide a region of vacuum within 1 μm of the area of interest for electron holography; (c) final milling from the top using an ion current of 150 pA to a membrane thickness of below 500 nm; (d) cuts at the sides of the membrane to relieve strain.

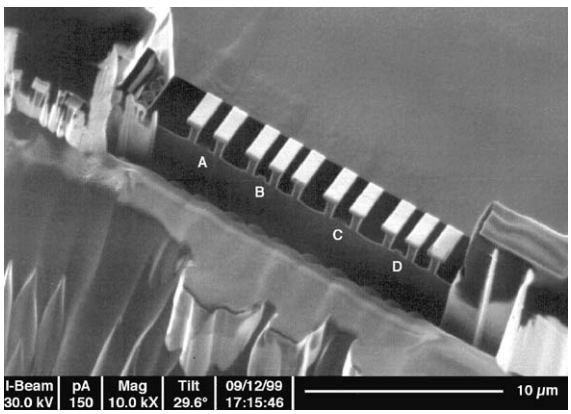

Fig. 3. FIB image showing an intermediate stage (corresponding to Fig. 2b) of conventional 'trench' specimen preparation of the transistor sample examined in this study. A, B, C and D are PMOS (0.5 μm gate), PMOS (0.35 μm gate), NMOS (0.5 μm gate) and NMOS (0.35 μm gate) transistors, respectively. The bright bands above the transistors are W contacts.

source and drain region of each transistor is in excess of $10^{20}\,cm^{-3}$, although some deactivation of the dopant is expected at a concentration as high as this [4]. The n- and p-type source and drain regions in the transistors contain As and B dopants, respectively.

Bright-field TEM images of finished specimens of nominal thickness 400 and 150 nm are shown in Figs. 4a and b, respectively. Labels A, B, C and D are equivalent to those in Fig. 3, while E indicates the position of a cut in the thicker membrane to relieve strain. Some of the metallization has been left above the gates to minimize the implantation of Ga into the doped regions during milling. In these images, the W contacts and the W silicide gates appear dark, and an obvious feature is the presence of thickness corrugations ('curtaining') in the Si substrate, which is thicker beneath the W contacts than between them.

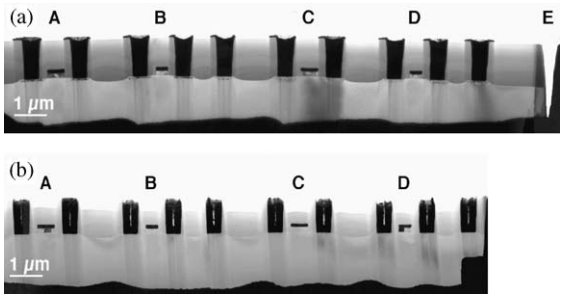

Fig. 4. Bright-field TEM images of finished FIB-milled 'trench' TEM specimens of nominal thickness (a) 400 nm and (b) 150 nm. A, B, C and D are PMOS (0.5 μm gate), PMOS (0.35 μm gate), NMOS (0.5 μm gate) and NMOS (0.35 μm gate) transistors, respectively. E shows a cut made to relieve strain. Note the thickness corrugations ('curtaining') visible in the Si substrate in each image. The gates are formed from W silicide, while the amorphous layers above the gates and between the W plugs are formed from Si oxides that have different densities.

Several holograms were required to cover the length of the row of transistors, and the resulting phase images had to be pasted together digitally during processing. A representative electron hologram, acquired from the PMOS (0.5 μm gate) transistor (A in Figs. 3 and 4) in the specimen of nominal thickness 400 nm, is shown in Fig. 5a. The fine fringes running from bottom left to top right are the holographic interference fringes, which carry information about the electrostatic potential in the specimen. The coarser fringes, of variable spacing, are Fresnel fringes from the edges of the biprism wire, while the black region at the bottom right corresponds to the specimen edge overlapped onto the Si substrate (the 'second image'). Fig. 5b shows a corresponding reference hologram, which was acquired from vacuum after the hologram of the specimen, and used during processing to remove artifacts in the phase images (such as geometrical distortions from the microscope lenses) associated with the imaging and recording process.

Results obtained from the specimen of nominal thickness 400 nm are shown in Fig. 6. A bright-field image of the PMOS (0.5 μm gate) transistor is included in Fig. 6a to show the locations of the regions analyzed in the subsequent figures. Faint horizontal bands of contrast with different gray levels between the W contacts are associated with

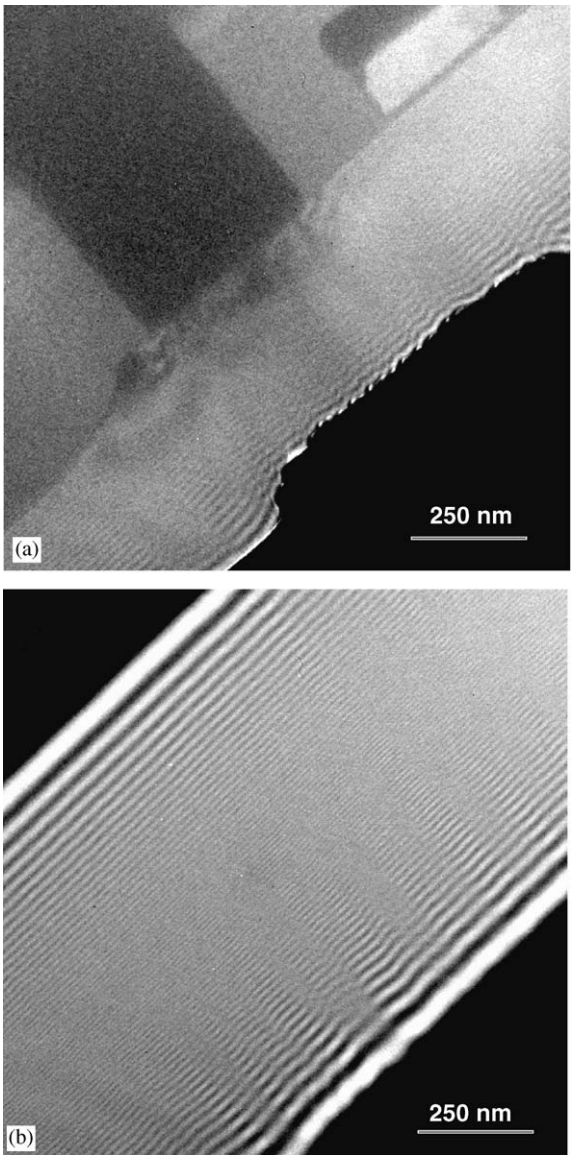

Fig. 5. (a) Representative off-axis electron hologram acquired from the PMOS (0.5 μm gate) transistor, marked 'A' in Figs. 3 and 4, in a 'trench' specimen of nominal thickness 400 nm. A microscope accelerating voltage of 200 kV and a biprism voltage of 160 V were used to acquire the hologram. The fine fringes running from bottom left to top right are the holographic interference fringes, which carry information about electrostatic (and magnetic) fields in the specimen. The coarser fringes, of variable spacing, are Fresnel fringes from the edges of the biprism wire. The black region at the bottom right corresponds to the specimen edge overlapped onto the Si substrate (the so-called 'second image'). Note the limited field of view and the strain contrast below the W contact. (b) Reference hologram acquired from vacuum immediately after acquiring the hologram of the specimen.

the presence of Si oxide layers of different density. Fig. 6b shows eight times amplified phase contours (i.e., the cosine of eight times the measured phase shift) from the region marked '1' in Fig. 6a. Surprisingly, instead of the expected phase distribution, which should be proportional to the mean inner potential multiplied by the specimen thickness, elliptical contours are visible in each Si oxide region, and a clear electrostatic fringing field is present outside the specimen edge (at the top of Fig. 6b). Both the elliptical contours and the fringing field are associated with the build-up of charge in the Si oxide in the electron microscope. The sense of the phase shift indicates that the oxide is positively charged, which is consistent with the emission of secondary electrons from the specimen during electron irradiation. Although care is required with interpretation of this image because it is formed from the projection of a three-dimensional electrostatic field both within and around the specimen, the maximum charge density appears to be several hundreds of nm from the specimen edge, approximately half-way between each pair of W contacts. Curiously, no substantial charge appears to have built up within or around the contacts themselves. Although the details in Fig. 6b will be affected by the use of a reference wave that is perturbed by the fringing field (note in particular the proximity of the second image in Fig. 5a) [21], the basic features are almost certainly correct.

Fig. 6c shows a similar phase image obtained after coating the specimen on one side with approximately 20 nm of carbon. The effects of charging are now entirely absent, there is no fringing field outside the specimen edge, and the

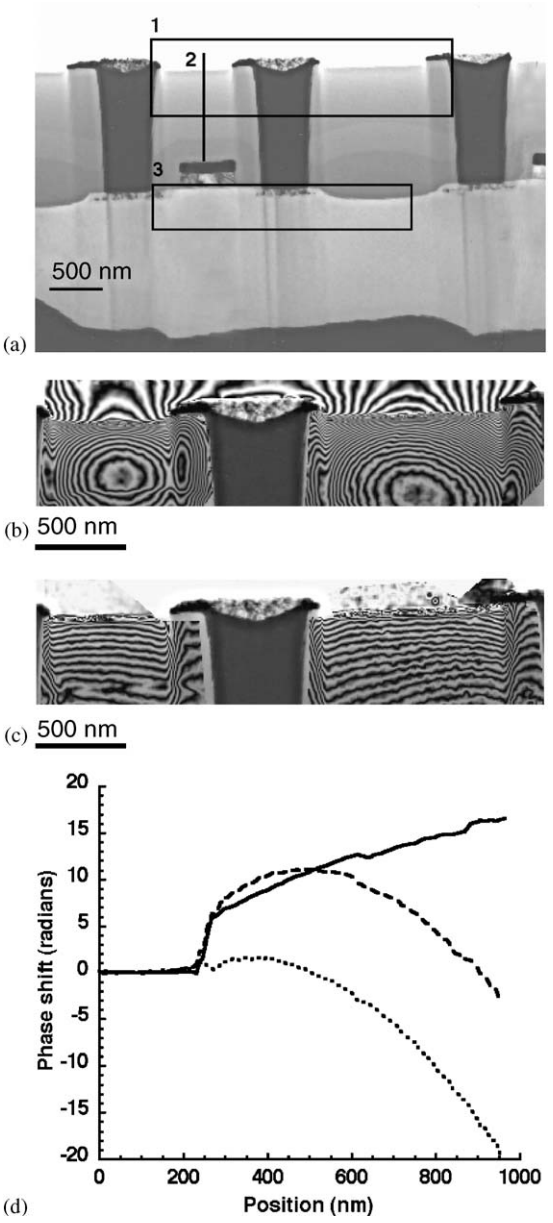

Fig. 6. Results obtained from the 'trench' specimen of nominal thickness 400 nm. (a) Bright-field TEM image of the PMOS (0.5 μm gate) transistor, indicating the locations of the regions analyzed in more detail in the subsequent figures. (b) Eight times amplified phase contours, calculated by combining phase images from several holograms obtained across the region marked '1' in (a). Specimen charging results in the presence of electrostatic fringing fields in the vacuum region outside the specimen edge, as well as elliptical phase contours within the Si oxide layers between the W contacts. (c) Shows an equivalent phase image obtained after coating the specimen on one side with approximately 20 nm of carbon to remove the effects of charging. The phase contours now follow the expected mean inner potential contribution to the phase shift in the oxide layers, and there is no electrostatic fringing field outside the specimen edge. (d) Shows one-dimensional profiles obtained from the phase images in (b) and (c) along the line marked '2' in (a). The dashed and solid lines were obtained before and after coating the specimen with carbon, respectively. The dotted line shows the difference between the solid and dashed lines.

phase contours in the specimen follow the change in specimen thickness in the oxide layers. One-dimensional profiles were generated from the phase images used to form Figs. 6b and c along the line marked '2' in Fig. 6a, and are shown in Fig. 6d. The dashed and solid lines correspond to results obtained before and after coating the specimen with carbon, respectively, while the dotted line shows the difference between the solid and dashed lines. As noted elsewhere [12], in a Si specimen that is charging as a result of secondary electron emission the phase shift starts to increase with specimen thickness on entering the specimen from vacuum but then decreases rapidly with increasing distance. In Fig. 6d, the dotted line (corresponding to charging alone) is flat in vacuum and then has a maximum gradient of approximately 0.06 rad per nm in the specimen. However, the vacuum phase is flat only because this profile has been calculated relative to a reference wave, whereas a line charge (e.g., along the edge of a specimen) is classically expected to have a more symmetrical, triangular phase profile. After correcting the phase gradient in this manner, the maximum phase gradient is approximately 0.03 rad per nm. The solid line in Fig. 6d suggests that the specimen thickness in this region (where the phase shift relative to vacuum is 15 rad) is ~200 nm, on the assumption that the mean inner potential of the oxide is 10 V [22]. If the charge is assumed to be distributed throughout the thickness of the specimen, then the electric field in the oxide (the phase gradient divided by $C_E t$) is approximately 2×10^7 V/m. This value is just below the breakdown electric field for thermal SiO_2 of 10^8 V/m [4].

Fig. 7 shows equivalent results obtained from the specimen of nominal thickness 150 nm, from both the PMOS (0.5 μm gate) and the PMOS

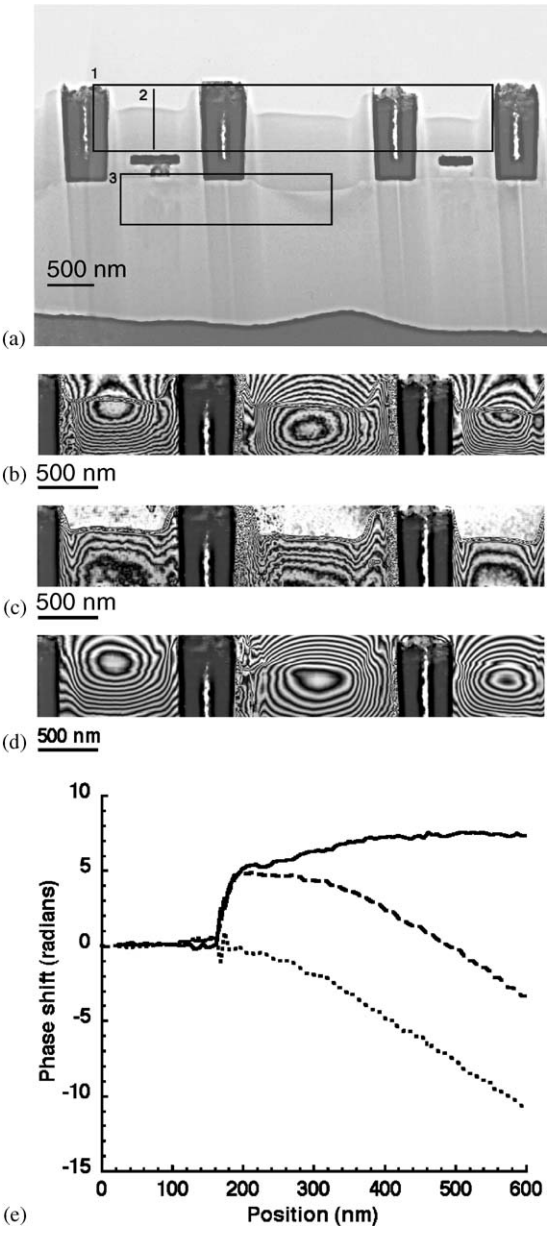

Fig. 7. As for Fig. 6 but for both the PMOS (0.5 μm gate) and the PMOS (0.35 μm gate) transistors in the 'trench' specimen of nominal thickness 150 nm. (a) Shows a bright-field TEM image of the transistors, indicating the locations of the regions analyzed in more detail. (b) and (c) show eight times amplified phase contours calculated from electron holograms of the region marked '1' in (a), before and after coating the specimen on one side with approximately 20 nm of carbon, respectively. (d) Shows the difference between phase images acquired before and after coating the specimen with carbon, again in the form of eight times amplified phase contours. (e) Shows one-dimensional profiles obtained from phase images along the line marked '2' in (a). The dashed and solid lines were obtained before and after coating the specimen with carbon, respectively. The dotted line shows the difference between the solid and dashed lines.

(0.35 μm gate) transistor. Fig. 7a shows a bright-field image of the transistors, while Figs. 7b and c show eight times amplified phase contours obtained from region '1' in Fig. 7a before and after coating the specimen with carbon, respectively. The phase contours are very similar to those shown for the thicker specimen in Fig. 6. The major difference is that in Fig. 7b the charge in the oxide peaks closer to the specimen edge than in Fig. 6b. Fig. 7d shows the difference between the phase images acquired before and after coating the specimen with carbon, again in the form of eight times amplified phase contours. One-dimensional profiles, obtained from the phase images along line '2' in Fig. 7a, are shown in Fig. 7e. As in Fig. 6, the dashed and solid lines correspond to results obtained before and after coating the specimen with carbon, respectively, while the dotted line shows the difference between the solid and dashed lines. By using a similar procedure to that described for Fig. 6 above, the thickness of the oxide in this region is estimated to be 100 nm, and the electric field is again inferred to be approximately 2×10^7 V/m.

Although only the oxide layers are considered in detail in Figs. 6 and 7, the effect of specimen charging on the dopant potential (in the source and drain regions of the transistors) is just as significant. The phase gradient in Figs. 6d and 7e continues into the Si substrate, and the dopant potential is always undetectable before carbon coating, whether or not a phase ramp is subtracted from the recorded images. For the transistors examined in this study, carbon coating is essential in order to image the dopant potential (see below) when conventional FIB milling is used to prepare the specimen.

The remaining problem is associated with the presence of thickness corrugations in the Si substrate. A simple approach for removing these thickness variations is illustrated in Figs. 8 and 9. Fig. 8a shows a montage of phase images acquired from region '3' in Fig. 6a, in the specimen of nominal thickness 400 nm, after carbon coating. The thickness corrugations are prominent, and the p-type region below the W contact is barely visible as a region of faint dark contrast close to the center of the image. As the thickness corrugations are approximately straight, they can be inferred from the Si substrate below the doped region and back-projected across the entire image, as shown in Fig. 8b. This image can then be subtracted from the original phase image to provide the difference image shown in Fig. 8c. The doped region is now visible more clearly.

By making use of Eq. (4), the total specimen thickness in this region is calculated to be approximately 330 nm from the corresponding holographic amplitude image. The measured phase shift between the substrate and the doped region is 1.0 rad, suggesting (using Eqs. (1)–(3) that if the built-in voltage is 1.0 V [4] then the electrically active specimen thickness is 140 nm. The total (crystalline and amorphous) electrically inactive

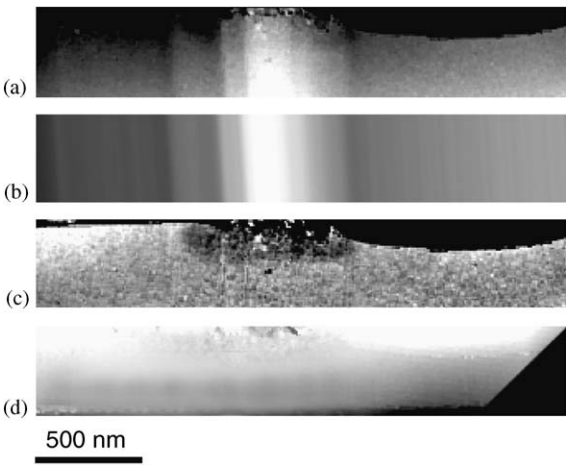

Fig. 8. Montage of phase images acquired from the region marked '3' in Fig. 6a, in the 'trench' specimen of nominal thickness 400 nm. (a) Shows thickness corrugations associated with 'curtaining' after coating the specimen with carbon [Black = 0, White = 9 rad]. The p-type-doped region below the W contact is just visible as a region of faint dark contrast close to the center of the image. (b) Shows the thickness corrugations alone, inferred from the Si substrate below the doped region at the bottom of the image in (a) [Black = 0, White = 9 rad]. (c) Shows the difference between the images in (a) and (b), illustrating one approach for removing the effects of 'curtaining' from recorded phase images. The doped region is now visible more clearly than in (a) [Black = 0, White-2.5 rad]. (d) Shows the result of applying the same approach before coating the specimen with carbon. There is now a steep gradient in phase from the top to the bottom of the image, and the doped region is not visible, either before or after 'flattening' the phase image [Black = 0, White = 20 rad].

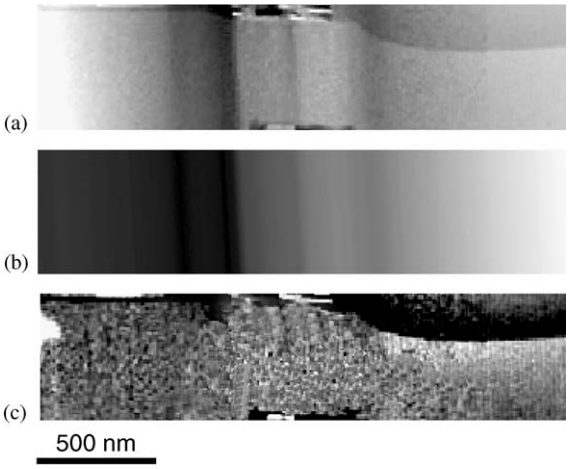

Fig. 9. As for Fig. 8 but for the 'trench' specimen of nominal thickness 150 nm. (a) Shows thickness corrugations associated with 'curtaining' after coating the specimen with carbon [Black = 0, White = 12 rad]. (b) Shows the thickness corrugations alone, inferred from the Si substrate below the doped region at the bottom of the image in (a) [Black = 0, White-12 rad]. (c) Shows the difference between the images in (a) and (b) [Black = 0, White = 1.5 rad].

thickness on each surface of the specimen is therefore 95 nm, slightly larger than previous reports for FIB-milled specimens (e.g. [13]). The contribution to this thickness from physical damage (amorphization) is expected to be between 20 and 30 nm [11]. Fig. 8d shows the result of applying the same approach before carbon coating. As mentioned above, there is now a steep gradient in phase from the top to the bottom of the image, and the doped region is not visible, either before or after removing a ramp from the image.

The importance of choosing a sufficiently large specimen thickness is illustrated in Fig. 9, which shows similar results obtained from the thinner FIB-milled specimen, of nominal thickness 150 nm, after carbon coating. The thickness of the doped region in this specimen was measured to be 110 nm from the holographic amplitude image. The original phase image, the thickness corrugations alone, and the difference between these images are shown in Figs. 9a–c, respectively. Dopant contrast is not visible in Fig. 9c because the specimen is too thin. The combined thickness of the electrically dead layers on the specimen surfaces is now comparable to the total specimen thickness.

3.2. Back-side milling

A more direct approach for overcoming the presence of thickness corrugations beneath the transistors involves FIB milling the specimen from the substrate side of the wafer ('back-side milling'). The specimen must be repositioned in the FIB workstation more often during milling than for the trench approach discussed above. However, this repositioning can be achieved relatively easily by mounting the specimen on a semicircular Cu grid in the geometry shown in Fig. 10.

In this geometry, a slice of wafer is prepared with the transistors close to its end. As for the trench technique, pre-grinding the specimen (to minimize both its height and its width) minimizes the amount of milling required. The specimen is initially milled from the side using a high beam current (11 nA) to leave a 20-μm-long, 5-μm-thick slab, as shown schematically in Fig. 10b. Conventional top-down milling is then used to locate the transistors at the center of a 1.5-μm-thick slice, as shown in Fig. 10c. A further stage of milling from the side is carried out (Fig. 10d) using a beam current of 350 pA to remove the metallization layers. Finally, milling from the substrate side is used to form a membrane whose final thickness is below 500 nm, and which has no corrugations. As for the trench technique, the specimen surface may be cleaned using low-energy Ar-ion milling in a Gatan PIPS. In the present study, Ar-ion milling was carried out for 2 min at 2 kV, without rotating the specimen, at an incident angle of ~25°.

Fig. 11a shows a low magnification bright-field image of a back-side-milled TEM specimen containing the four transistors. A higher magnification bright-field image of the membrane, whose thickness is approximately 500 nm, is shown in Fig. 11b. A bright-field image of the same membrane after further FIB milling from the substrate side of the specimen is shown in Fig. 11c. In this image, the specimen thickness close to transistors A and B is approximately 250 nm. A Pt strap was not used during back-side milling, and as a result a 700-nm-thick amorphous layer, which is

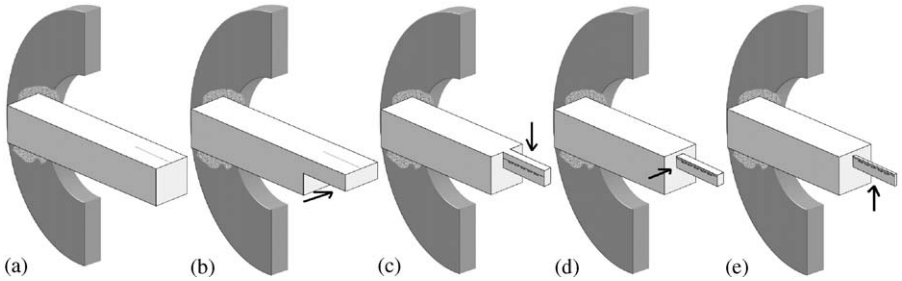

Fig. 10. Schematic diagrams illustrating a 'back-side-milling' approach for preparing TEM specimens of transistors using FIB milling. The stages involved include: (a) mounting the specimen on a semi-circular 3-mm-diameter Cu ring, with the transistors close to the end of the slab; (b) milling away the bottom (substrate side) of the end of the specimen using a high beam current of 11 nA, to leave an approximately 20-μm-long, 5-μm-thick slab; (c) top-down milling to form a 1.5-μm-thick membrane; (d) milling from the side to remove the passivation and metallization layers close to the wafer surface; (e) milling the specimen from the Si substrate side to a thickness of below 500 nm.

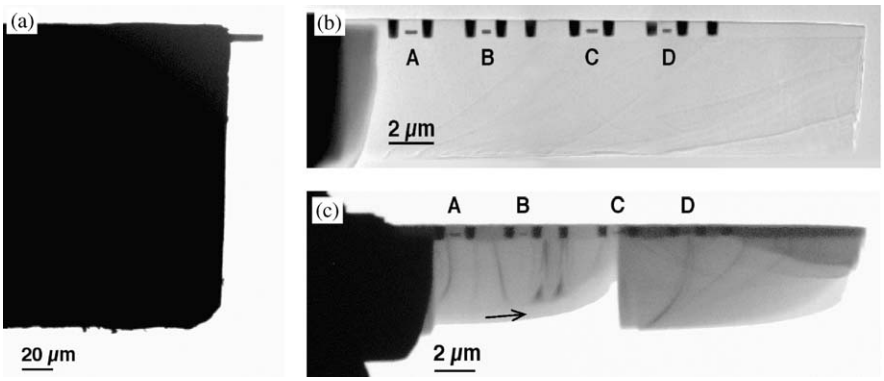

Fig. 11. (a) Low magnification bright-field image showing a back-side-milled TEM specimen containing the transistors examined in this study. (b) Higher magnification bright-field image of the membrane, whose thickness is approximately 500 nm. (c) Bright-field image of the membrane after further milling from the substrate side. The specimen thickness close to transistors A and B is approximately 250 nm. An approximately 700-nm-thick amorphous layer is highlighted using an arrow at the bottom of the thinnest membrane in (c). The surface of the specimen shown in (c) was cleaned by using low-angle Ar-ion milling in a Gatan PIPS after FIB milling.

identified by the absence of bend contours in Fig. 11c, is present in the thinnest specimen.

The geometry of the specimen shown in Fig. 11c is illustrated in more detail in Fig. 12, which shows five members of a tilt series of high-angle annular dark field images. The images correspond to nominal specimen tilt angles of $+74^\circ$, $+40^\circ$, 0°, -40° and -74°, and are taken from a series that was acquired in steps of 2°. The damaged layer at the bottom of the slice is visible clearly, and no thickness corrugations are apparent in the Si substrate. Slight bending of the membrane is visible directly in Fig. 12e. The result of a tomographic reconstruction of the entire tilt series [23] is shown in Fig. 13a, with the contrast inverted for display purposes. The vertical streaks that are visible in the Si substrate below the W contacts are artifacts, which result from the high atomic number and thickness of the contacts, in which the signal is no longer proportional to specimen thickness. The thickness profile of the membrane is shown in Fig. 13b in the form of a contour of constant density. Fig. 13c shows a vertical section extracted from the reconstructed volume at the

position of the slice in Fig. 13b, while Fig. 13d shows a corresponding intensity profile along the line shown in Fig. 13c. The change in density at the thick damaged layer and a narrower low-density layer on each of the flat specimen surfaces are visible in Fig. 13c. The localized region of bright contrast at the very base of the slice in Fig. 13c, which is also visible on the right of Fig. 13d, is likely to be associated with the presence of a high concentration of implanted Ga. (The bright contrast at the top of Fig. 13c corresponds to the edge of a W contact next to the slice extracted from the reconstruction.)

Fig. 14 shows a montage of electron holographic phase images acquired from the PMOS (0.5 μm gate) and the PMOS (0.35 μm gate) transistors in the thinnest back-side-milled specimen shown in Fig. 11c. The thickness of the doped regions in this specimen was determined to be 330 nm from the holographic amplitude image. Each doped region is clearly visible in the measured phase image. Surprisingly, carbon coating is now not required to prevent specimen charging, presumably because of the sputtering and subsequent redeposition of Si onto the oxide layers between the W contacts during FIB milling. Some diffraction contrast is present in the Si substrate in Fig. 14a in addition to the dopant contrast of interest. Coating the specimen with carbon now has the unexpected disadvantage of introducing strain into the thin specimen, which is visible in Fig. 14b in the form of bright regions that result from local variations in diffraction contrast across bend contours. A line profile obtained from the phase image of the back-side-milled specimen along the line shown in Fig. 14a (before coating with carbon) is shown in Fig. 14c. The phase change of 0.8 rad suggests that the electrically active specimen thickness is 110 nm, on the assumption of a built-in voltage of 1.0 V.

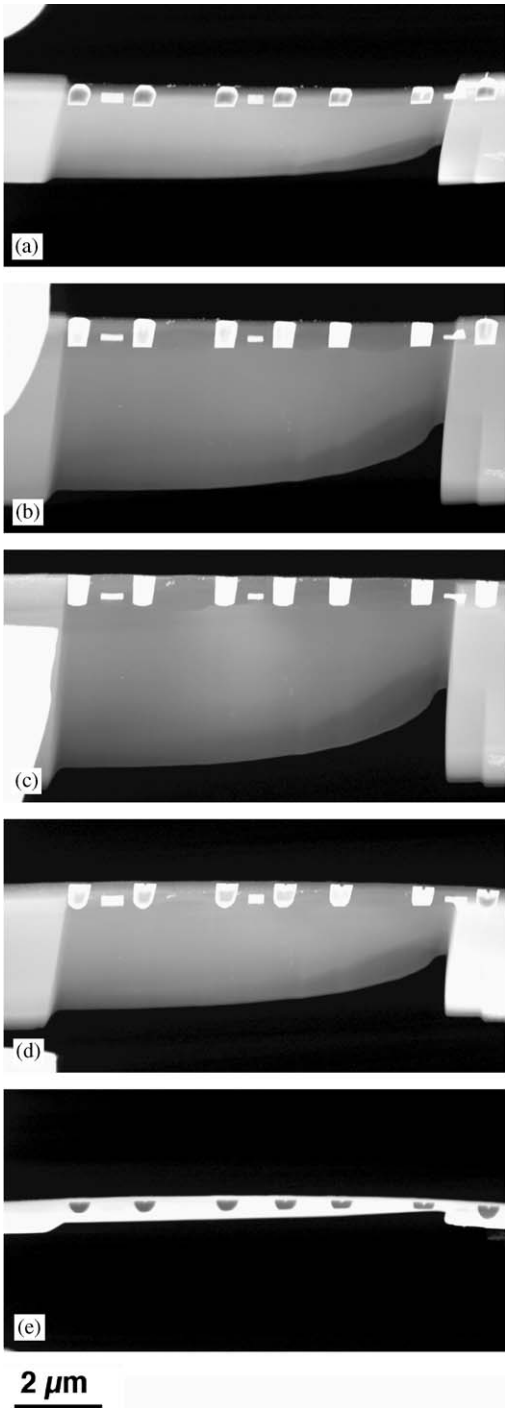

Fig. 12. Five members of an ultra-high-tilt series of high-angle annular dark field images of the back-side-milled specimen shown in Fig. 11c. The images were acquired in steps of 2° at 200 kV in a Tecnai F20 FEGTEM using a 0.7-nm-diameter probe, a 20 s acquisition time and a pixel resolution of 6 nm/pixel. The images shown correspond to nominal tilt angles of (a) +74°; (b) +40°; (c) 0°; (d) −40°, and (e) −74°. The inner angle of the detector used was in excess of 50 mrad.

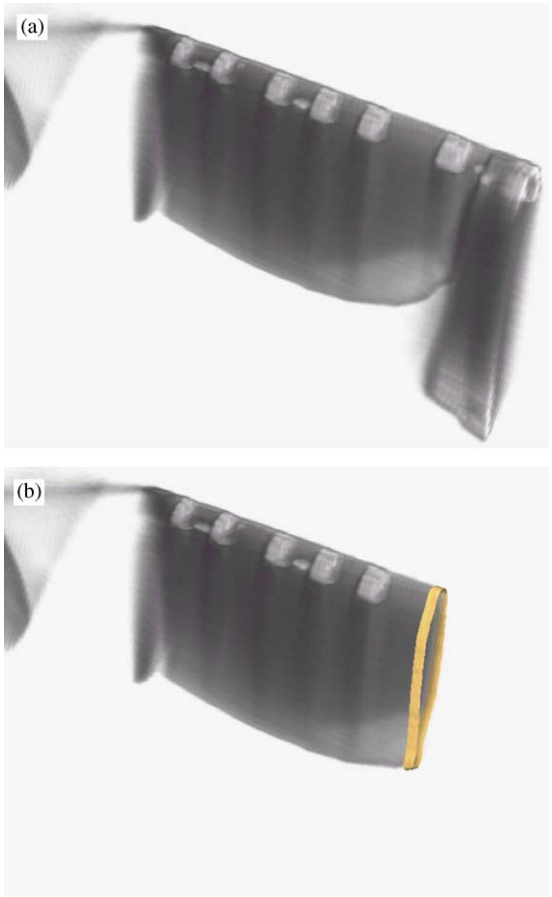

Fig. 13. (a) Tomographic reconstruction of the tilt series of images illustrated in Fig. 12, shown with inverted contrast. The vertical streaks that are visible in the Si substrate below the W contacts are artifacts of the reconstruction, which result from their high atomic number and thickness (and therefore a signal that is no longer proportional to specimen thickness). (b) The reconstruction cropped to illustrate the specimen thickness profile of the slice. The yellow band shows a contour of constant density. (c) Vertical section through the reconstruction, extracted at the position of the yellow band in (b). (d) Intensity profile extracted along the line shown in (c).

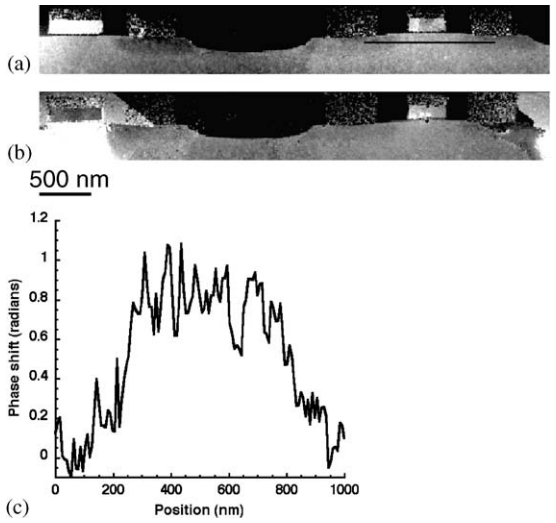

Fig. 14. (a) Montage of phase images obtained from the PMOS (0.5 μm gate) and the PMOS (0.35 μm gate) transistors in the back-side-milled specimen shown in Figs. 11c, 12 and 13 [Black = 0, White = 3 rad]. Some diffraction contrast is visible in the Si substrate in addition to the dopant potential of interest. (b) As for (a) but after coating the specimen with approximately 20 nm of carbon [Black = 0, White = 5 rad]. The bright regions in the substrate on the left and right sides of the image result from local variations in diffraction contrast across bend contours. (c) Line profile obtained from the phase image of the back-side-milled specimen before coating with carbon, along the line shown in (a).

The total electrically inactive specimen thickness on each surface is therefore 110 nm, which is comparable to the value measured for the trench specimen described above. This value was found to be unaffected by carbon coating.

4. Discussion and conclusions

Conventional FIB milling of a semiconductor device that has metallization layers on its surface results in thickness corrugations in the doped region beneath, which strongly affect phase images recorded using off-axis electron holography. One solution, which is described with reference to the trench technique above, is to determine the one-dimensional thickness variation from the region far below the source and drain of the transistor

and then to remove this corrugation from the entire image to leave the dopant potential of interest. The alternative approach of back-side FIB milling provides a more convenient approach for overcoming curtaining effects (thickness corrugations) when examining the source and drain regions of semiconductor transistors, as well as allowing a hole to be micro-machined close to the region of interest for electron holography. Although FIB milling from a number of different directions is then required, this requirement can be achieved relatively easily if the specimen is mounted in a specific orientation on a semi-circular Cu grid. An unexpected additional benefit of using back-side milling is that charging of the specimen due to secondary electron emission, which was observed when preparing the same specimen using more conventional 'trench' FIB milling, no longer occurs. Deposition of carbon is then found to be disadvantageous as it results in bending of the specimen. This difference in the charging properties of the specimen presumably results from the extent of Si redeposition onto the specimen surface during FIB milling. Although a significant electrically inactive layer was found to be present on the surfaces of both conventionally prepared and back-side FIB-milled specimens, this dead layer thickness may be minimized in future studies by using a suitable combination of Pt deposition, Ar-ion milling and perhaps also low-temperature annealing.

Our study can be compared with that of Schwarz et al. [24], who eliminated curtaining effects by using a lift-out procedure to mount a transistor specimen onto one side of a Cu grid with ion-beam-assisted Pt deposition, and subsequently milled this specimen from the substrate side of the device. The FIB workstation was then also used to remove material close to the gate in order to provide a reference wave for electron holography, and Ar-ion milling was used to remove the FIB damage. McCartney et al. [25] provide an overview of this and other techniques for the preparation of semiconductor devices for electron holography.

Charging of oxide layers in the trench specimens, and in particular the presence of electrostatic fringing fields outside the specimen surfaces, is unexpected because fringing fields have never been observed outside FIB-milled semiconductor specimens that contain p–n junctions [13], or outside chemically thinned specimens until they are reverse-biased [26]. Our results suggest that when substantial oxide layers are present the specimen surfaces in these regions are no longer equipotentials after FIB milling and electron irradiation, unless Si is sputtered and redeposited onto the specimen surface (as in back-side milling). The presence of positively charged surface oxide layers has been used by Beleggia et al. [27] to explain anomalous phase contrast from p–n junctions. An extensive comparison of off-axis holography results with first principles computer simulations of the three-dimensional potential in a TEM sample of arbitrary geometry, with arbitrary surface states and boundary conditions, is also required. Such studies, which are in progress both within our research group [28] and elsewhere [29], should allow the effect of TEM specimen preparation on the nature of the surface of the TEM specimen to be understood fully.

Acknowledgments

We are grateful to D. Doyle and A. Deignan at Analog Devices in Limerick, Ireland, for fabricating the transistor specimen, J. Li for useful discussions, and the Royal Society, FEI and the Isaac Newton Trust for supporting this work. We acknowledge the use of electron microscopy facilities at the Center for High-Resolution Electron Microscopy at Arizona State University.

References

[1] R.E. Dunin-Borkowski, M.R. McCartney, D.J. Smith, Electron holography of nanostructured materials, in: H.S. Nalwa (Ed.), Encyclopaedia of Nanoscience and Nanotechnology, vol. 3, American Scientific Publishers, Stevenson Ranch, CA, 2004, pp. 41–100.
[2] A. Tonomura, L.F. Allard, G. Pozzi, D.C. Joy, Y.A. Ono (Eds.), Electron Holography, Elsevier, Amsterdam, 1995.
[3] E. Völkl, L.F. Allard, D.C. Joy (Eds.), Introduction to Electron Holography, Plenum, New York, 1998.
[4] S.M. Sze, Physics of Semiconductor Devices, Wiley, New York, 2002.

[5] D.M. Donnet, A.E.M. De Veirman, B. Otterloo, H. Roberts, Paper presented at Microscopy of Semiconducting Materials, Cambridge, 2003, Inst. Phys. Conf. Ser. 180 (2003) 617.
[6] Z. Wang, T. Hirayama, K. Sasaki, H. Saka, N. Kato, Appl. Phys. Lett. 80 (2002) 246.
[7] Z. Wang, T. Kato, N. Shibata, T. Hirayama, N. Kato, K. Sasaki, H. Saka, Appl. Phys. Lett. 81 (2002) 478.
[8] Z. Wang, T. Kato, T. Hirayama, K. Sasaki, H. Saka, N. Kato, J. Vac. Sci. Technol. B 21 (2003) 2155.
[9] T. Ishitani, H. Koike, T. Yaguchi, T. Kamino, J. Vac. Sci. Technol. B16 (4) (1998) 1907.
[10] R.M. Langford, A.K. Petford-Long, J. Vac. Sci. Technol. A 19 (2001) 2186.
[11] D. Sutton, S.M. Parle, S.B. Newcomb, Inst. Phys. Conf. Ser. 168 (2001) 377.
[12] M.R. McCartney, M.A. Gribelyuk, J. Li, P. Ronsheim, J.S. Mcmurray, D.J. Smith, Appl. Phys. Lett. 80 (2002) 3213.
[13] A.C. Twitchett, R.E. Dunin-Borkowski, P.A. Midgley, Phys. Rev. Lett. 88 (2002) 238302.
[14] M.A. Gribelyuk, M.R. McCartney, J. Li, C.S. Murthy, P. Ronsheim, B. Doris, J.S. McMurray, S. Hegde, D.J. Smith, Phys. Rev. Lett. 89 (2) (2002) 5502.
[15] W.D. Rau, P. Schwander, F.H. Baumann, W. Hoppner, A. Ourmazd, Phys. Rev. Lett. 82 (1999) 2614.
[16] R.E. Dunin-Borkowski, S.B. Newcomb, D. Doyle, A. Deignan, M.R. McCartney, in: J. Frank, F. Ciampor (Eds.), Proceedings of the 12th European Congress on Electron Microscopy, Czechoslovak Society for Electron Microscopy, Brno, 2000, pp. 163–164.
[17] W.O. Saxton, T.J. Pitt, M. Horner, Ultramicroscopy 4 (1979) 343.
[18] M. Gajdardziska-Josifovska, M.R. McCartney, Ultramicroscopy 53 (1994) 283.
[19] K.H. Park, Mater. Res. Soc. Symp. Proc. 199 (1990) 271.
[20] J. Szot, R. Hornsey, T. Ohnishi, J. Minagawa, J. Vac. Sci. Technol. B 10 (1992) 575.
[21] G. Matteucci, G.F. Missiroli, G. Pozzi, Adv. Imaging Electron Phys. 99 (1998) 171.
[22] Y.C. Wang, T.M. Chou, M. Libera, T.F. Kelly, Appl. Phys. Lett. 70 (1997) 1296.
[23] P.A. Midgley, M. Weyland, J.M. Thomas, B.F.G. Johnson, Chem. Commun. 10 (2001) 907.
[24] S.M. Schwarz, B.W. Kempshall, L.A. Giannuzzi, M.R. McCartney, Microsc. Microanal. 9 (Suppl. 2) (2003) 116.
[25] M.R. McCartney, J. Li, P. Chakraborty, L.A. Giannuzzi, S.M. Schwarz, Microsc. Microanal. 9 (Suppl. 2) (2003) 776.
[26] S. Frabboni, G. Matteucci, G. Pozzi, M. Vanzi, Phys. Rev. Lett. 55 (20) (1985) 2196.
[27] M. Beleggia, P.F. Fazzini, P.G. Merli, G. Pozzi, Phys. Rev. B 67 (2003) 045328.
[28] P.K. Somodi, R.E. Dunin-Borkowski, A.C. Twitchett, C.H.W. Barnes, P.A. Midgley, Inst. Phys. Conf. Ser. 180 (2003) 501.
[29] L. Houben, M. Luysberg, T. Brammer, Phys. Rev. B 70 (2004) 165313.